Precise Measurement of the Interstellar Flow with IMAP, Informed by IBEX Observations

SH13C-2964 **E. Möbius[1]**, N. Schwadron[1], M. Bzowski[2], S.A. Fuselier[3,4], D. Heirtzler[1], M.A. Kubiak[2], H. Kucharek[1], M.A. Lee[1], D.J. McComas[5], P. Swaczyna[5], J.M. Sokol[2], P. Wurz[6]

Contact: eberhard.moebius@unh.edu

[1]Space Science Center, University of New Hampshire, Durham, NH [2]Space Research Center Polish Academy of Sciences, Warszawa, Poland [3]Southwest Research Institute, San Antonio, TX

[4]University of Texas, San Antonio, TX [5]Department of Astrophysical Sciences, Princeton University, NJ [6]Physikalisches Institut, Universität Bern, Switzerland

Supported by:

NASA USA

PAS Poland

SNF Switzerland

Introduction

- The Interstellar Boundary Explorer (IBEX) obtains a precise relation between the interstellar neutral (ISN) flow longitude $\lambda_{ISN\infty}$ and speed $V_{ISN\infty}$, along with latitude $\beta_{ISN\infty}$ and temperature T_{ISN} in a 4D tube, with substantially larger uncertainty along the tube (**Fig. 1** [1, 2, 3, 4, 5]). The velocity vector $\mathbf{V}_{ISN\infty}$ is in agreement with Ulysses GAS [6, 7, 8], but with a higher temperature T_{ISN} from IBEX observations [1, 3, 4].
- The interstellar magnetic field $\mathbf{B}_{IS}$ from the IBEX ribbon, is consistent with the heliospheric asymmetry and TeV cosmic ray anisotropy [9].
- These vectors define the $\mathbf{B}_{IS}$- $V_{ISN\infty}$ plane, which controls the shape of and the flow deflection in the outer heliosheath [10, 11].
- Independent determination of $\lambda_{ISN\infty}$ (Poster SH13C-2954) along with tightening and tracking over time the parameter tube will refine the $\mathbf{B}_{IS}$- $V_{ISN\infty}$ plane and constrain potential temporal variations [12, 13, 14].

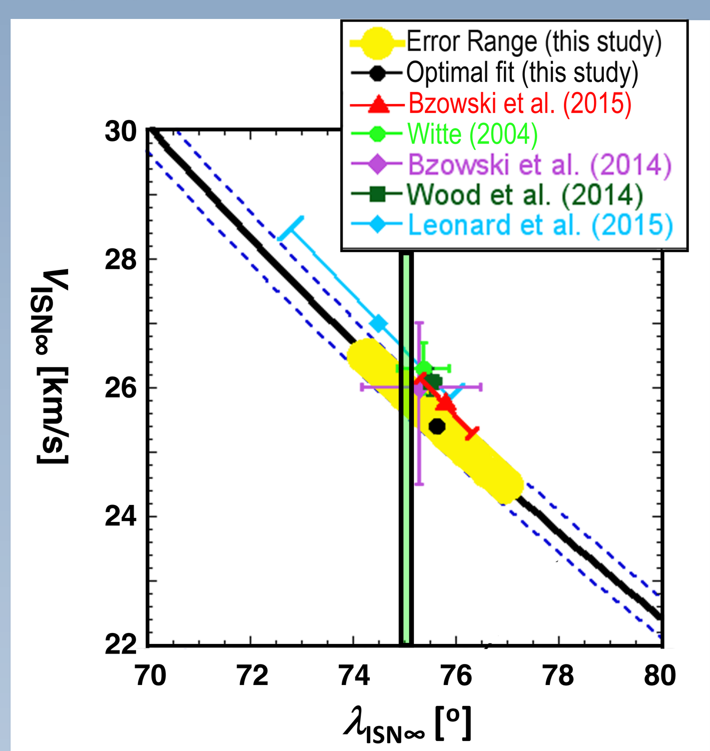

FIGURE 1: Relationship between $\mathbf{V}_{ISN\infty}$ and $\lambda_{ISN\infty}$ according to the IBEX parameter tube based on various IBEX analyses in comparison with Ulysses results (adapted from [5]). Also shown with a vertical bar is how an independent determination of $\lambda_{ISN\infty}$ will constrain the ISN flow vector.

ISN Parameter Tube and Flow Longitude

- **ISN Parameter Tube Determination:** $V_{ISN\infty}(\lambda_{ISN\infty})$ is determined by the ISN bulk flow longitude $\lambda_{ISN\ Peak}$ at 1 AU observed with IBEX [4, 15] (***discussed here***).
- **Flow Longitude Determination**: $\lambda_{ISN\infty}$ can be determined separately from the radial ISN flow speed V_r (or pickup ion cut-off) as a function of λ_{Ecl}, which is symmetric about $\lambda_{ISN\infty}$ [16, 17] (***systematic effects discussed on Poster SH13C-2954***).

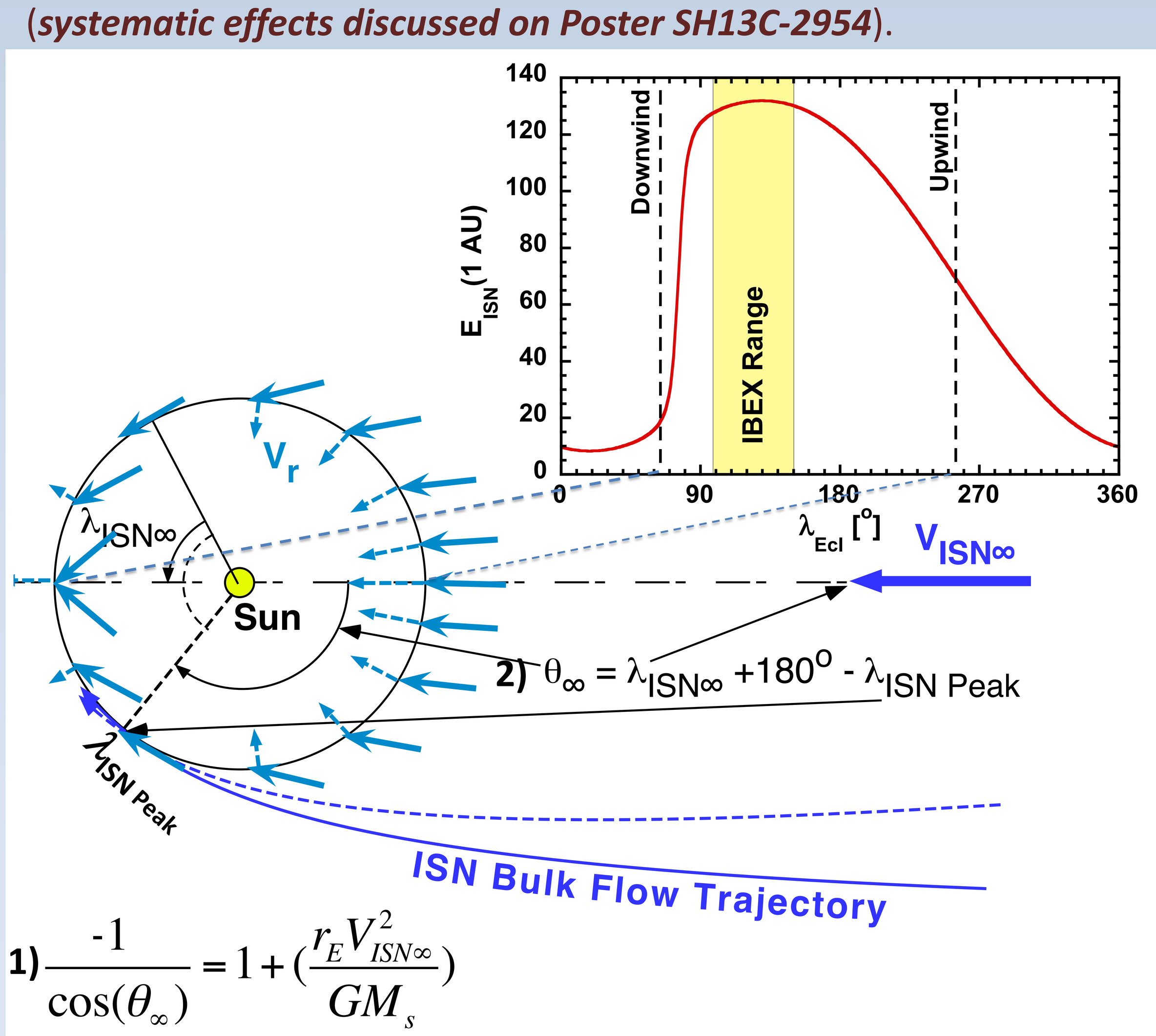

$$1)\ \frac{-1}{\cos(\theta_\infty)} = 1 + \left(\frac{r_E V_{ISN\infty}^2}{GM_s}\right)$$

FIGURE 2: Schematic view of sample ISN trajectories (dark blue) and flow vectors along Earth's orbit (light blue). The blue dashed line indicates an alternate Bulk Flow Trajectory that also belongs to the ISN parameter tube. Both satisfy eq. 1) and reach their perihelion at $\lambda_{ISN\ Peak}$, which is connected with $\lambda_{ISN\infty}$ and θ_∞ through eq. 2). The light blue dashed arrows indicate the pattern of V_r, which can be sensed by the pickup ion cut-off.

Spin-Integrated ISN Flux and In-Flight Calibration

Spin-integrated ISN rates are first used for in-flight validation of the relative IBEX-Lo calibration for He, which is detected through sputtered negative ions, mainly H⁻, with a schematic energy dependence (**Fig. 3, left**). After normalizing the ESA Step 1,2, 4 rates to the ESA Step 3 and the ESA energies to the mean ISN energy (**Fig. 2, inset**), the ratios (**Fig. 3, right**) behave similarly to the schematic curve, only with strong E-dependence for ESA Step 4. IMAP allows finer steps and extends validation for E_{ISN} = 10 – 135 eV (**Fig. 2**).

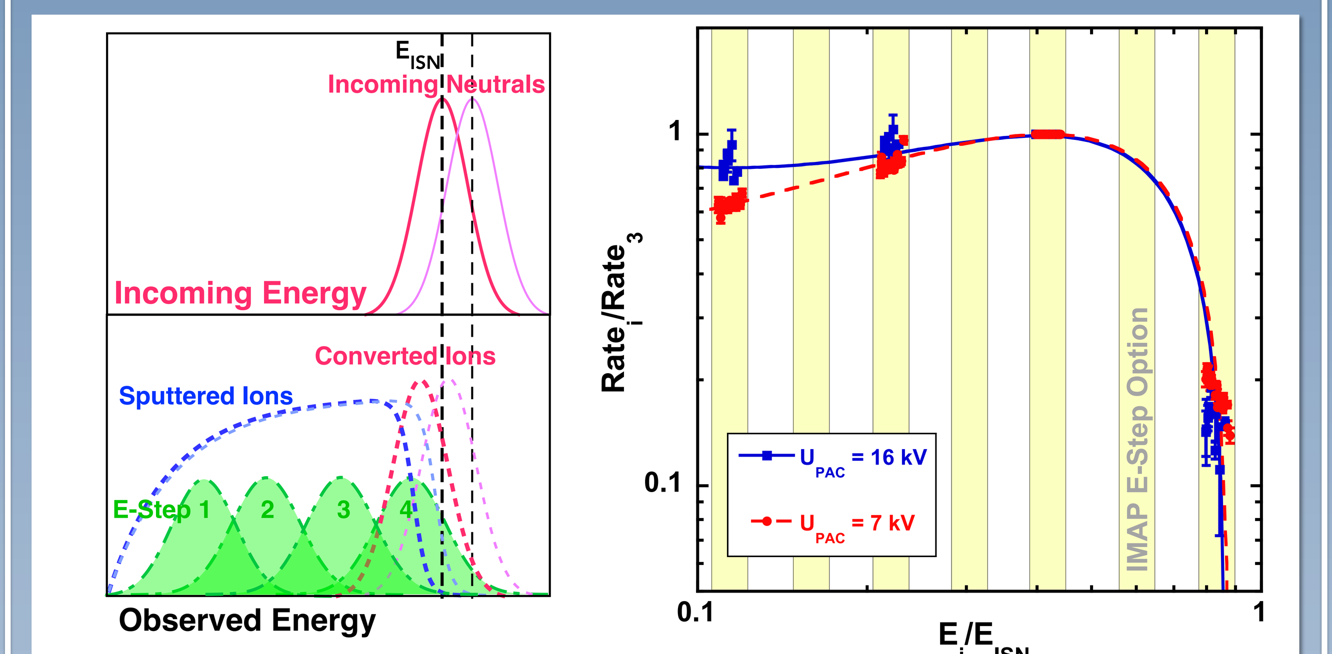

Figure 3: Left: Schematic view of expected processed ion energy distributions of incoming neutral atom distributions (top) for direct conversion to negative ions (red dashed line) or sputtered ions (blue dashed lines). The IBEX-Lo ESA Steps are indicated in green.
Right: Ratios of spin-integrated count rates (Rate$_i$/Rate$_3$), where i = 1,2,4, as a function of the ratio of the ESA Step center energy over the mean ISN energy in the S/C frame (E_i/E_{ISN}) for post acceleration voltage 16 kV (2009-2012, blue) and 7 kV (≥2013, red). The yellow bars indicate optional finer ESA Steps with IMAP-Lo.

Determination of the ISN Flow Peak Longitude

The determination of $\lambda_{ISN\ Peak}$ involves the following steps [17]:

- **ISN Good Times** for each IBEX orbit [2], but retain time intervals that are despun at ground because of missing Star Tracker pointing information
- **Spin Integrated ISN Count Rates** ±3σ of peak divided by σ per 512 spins
- **Linear Chi-Squared Fit to these Rates** as function of λ_{Ecl} (**see Fig. 4**)
  → obtain rate at λ_{Ecl} where IBEX spin points exactly at the Sun in λ or at specific angle ε_E from the Sun, adjusted for IBEX motion
- **Compensate Rates (see Fig. 3) for**
  - Observation of ISN flux, while ISN bulk flow corresponds to peak in Phase Space Density (PSD) of the ISN distribution → Flux∝ PSD x V^3
  - Extinction by ionization along trajectory in λ_{Ecl} using TIMED & SDO data.
  - Presence of Secondary He according simulations based on [18]

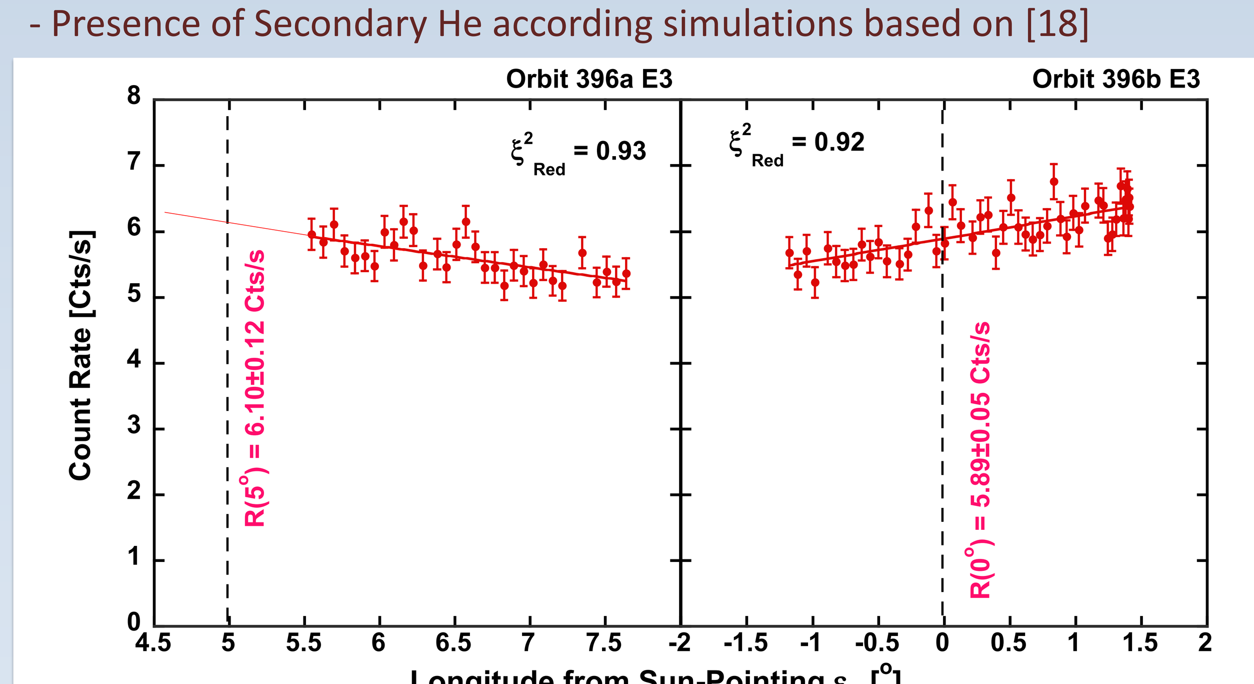

FIGURE 4: Spin-integrated count rates as a function of offset from Sun-pointing ε_E for Orbit 396 (ε_E = 0°: aberration corrected Sun-pointing) with linear Chi-squared fit to the observations and locations for further analysis in **Fig. 5**.

Uncertainties of Data for Each Orbit Contain:
- Fit error (x2 for restriction to linear and omission of curvature)
- Uncertainty in conversion to IBEX frame, using slope of Chi-squared fit and model Gaussian in **Fig. 5**)
- Uncertainties of compensation for secondary He and ionization

Determination of the ISN Flow Peak Longitude

To obtain a value for $\lambda_{ISN\ Peak}$ the adjusted rates from each IBEX orbit arc are evaluated for their variation with λ_{Ecl}. Usable orbits satisfy:
- Observations are within 110° ≤ λ_{Ecl} ≤ 160°
- Position at exact or ε_E from Sun-pointing of the spin axis is inside of or the extrapolation is less than the range of the data interval in λ_{Ecl}

Rates are Chi-squared fitted to a Gaussian for all 2013-2018 data after normalizing the rates to the peak rate.

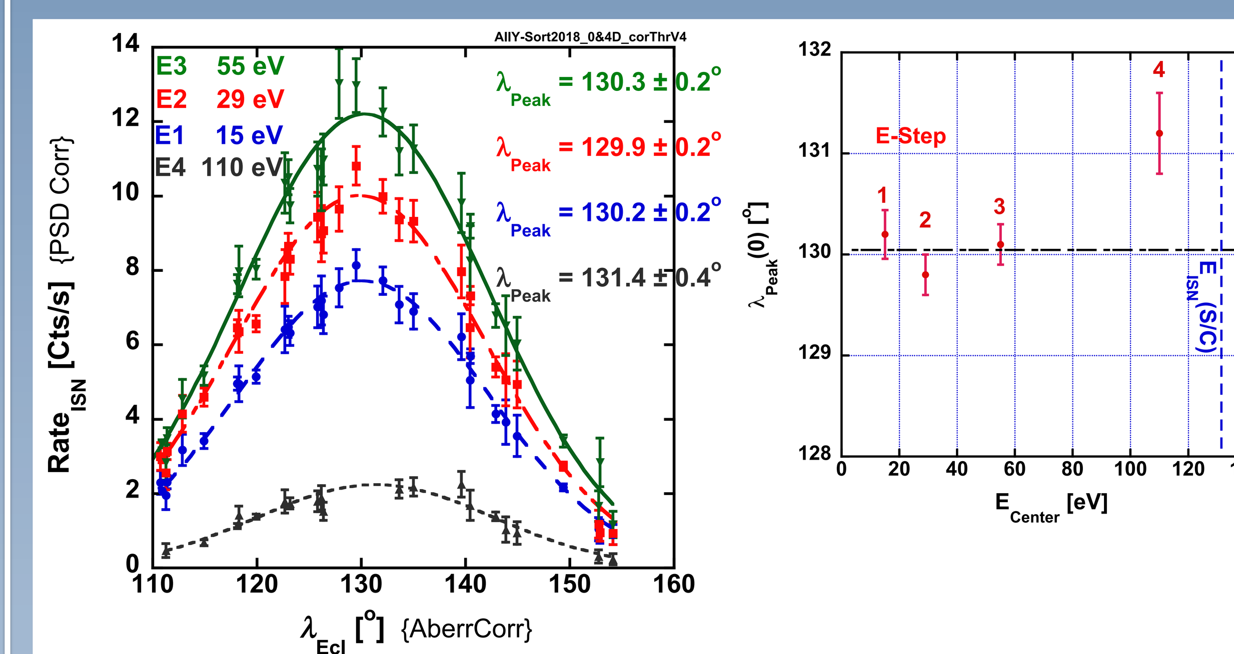

FIGURE 5: Left: Spin-integrated count rates of the He ISN flow, obtained in ESA Steps 1-4 at the location of exact Sun-pointing of the IBEX spin axis, corrected for aberration. The count rates have been transformed from flux to phase space density, adjusted for ionization loss and the presence of secondary He. Also shown are the Chi-squared fits to a Gaussian with the resulting peak longitudes.
Right: Peak longitudes with fit error bars as a function of ESA Step energy.

- $\lambda_{ISN\ Peak}$ for ESA Step 1-3 are identical within error bars
- ESA Step 4 is shifted by ~+1°
  consistent with E-dependence of relative efficiencies in **Fig. 3**
  → Use ESA Step 3 (with essentially *E*-independent efficiency **Fig. 3**) to evaluate $\lambda_{ISN\ Peak}$ for different offsets ε_E from Sun-Pointing

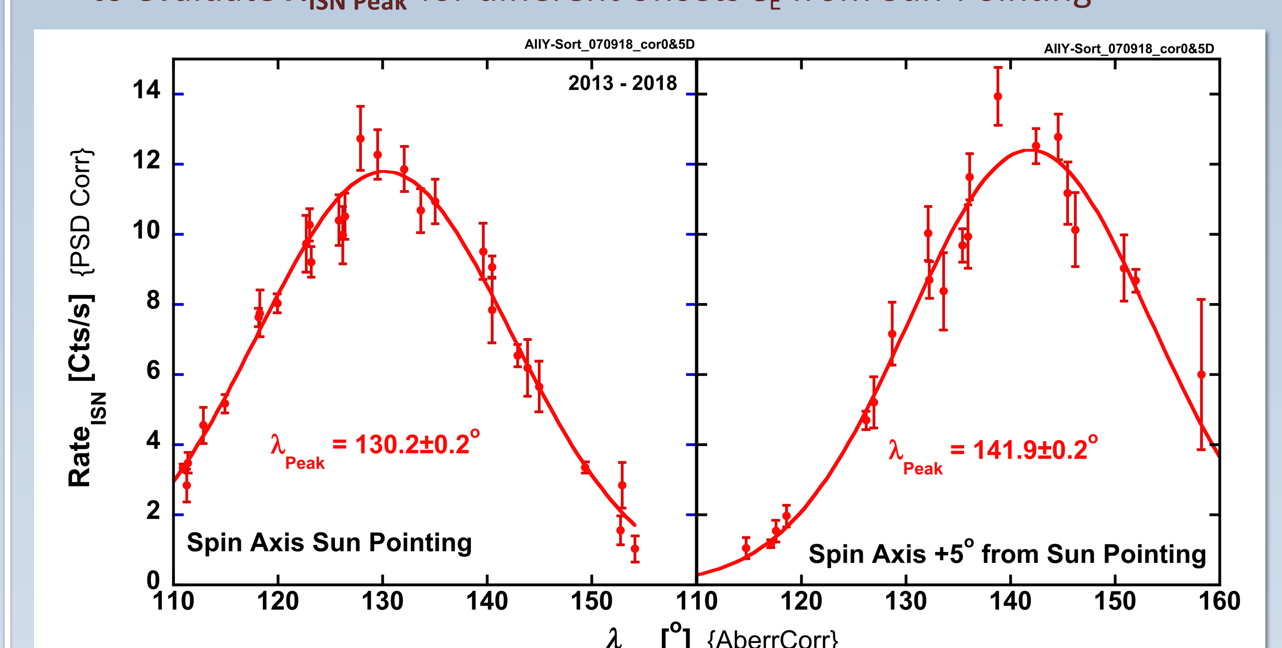

FIGURE 6: Spin-integrated count rates of the He ISN flow, obtained in ESA Steps 3 at the location of IBEX spin axis pointing exactly at the Sun, ε_E = 0° (left) and at angle ε_E = 5° west of the Sun (right), along with Chi squared fit to a Gaussian. The peak location is different by 12° in longitude.

ε_E as a function of $\lambda_{ISN\ Peak}$ (**Fig. 7**) follows the analytic curve for the ISN parameter tube with $V_{ISN\infty}$ = 25.5 km/s and $\lambda_{ISN\infty}$ = 75.6° [1,3,4,5]. Curves for different tubes differ, but stay within error bars for IBEX observations.

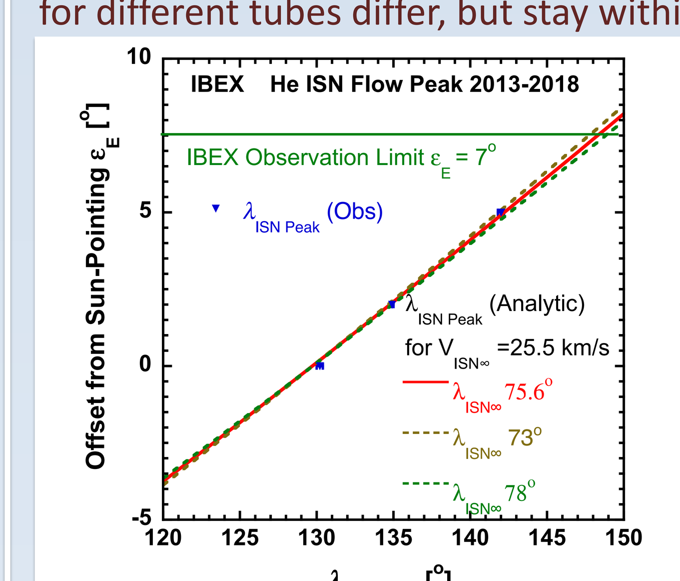

FIGURE 7 Offset ε_E from exact Sun-pointing of the spin axis as a function of $\lambda_{ISN\ Peak}$, based on observations (c.f. **Fig. 6**) and on analytic modeling for different ISN parameter tubes.

Crossing ISN Parameter Tubes with IMAP

- **Future Reduction of Systematic Effects with IMAP:**
  Different ISN parameter tubes cross at the actual ISN inflow longitude $\lambda_{ISN\infty}$, as shown for simulated tubes in **Fig. 8**. Parameter tubes for the pointing range of IBEX (up to 7° west of the Sun) provide only a weak constraint on $\lambda_{ISN\infty}$ (**Fig. 8**, left), consistent with larger error bars along the tube [1 – 5]. IMAP-Lo will be mounted on a Pivot Platform that allows pointing at the ISN flow over almost the entire orbit around the Sun. This will provide tubes crossing at large angles (**Fig. 8**, right).

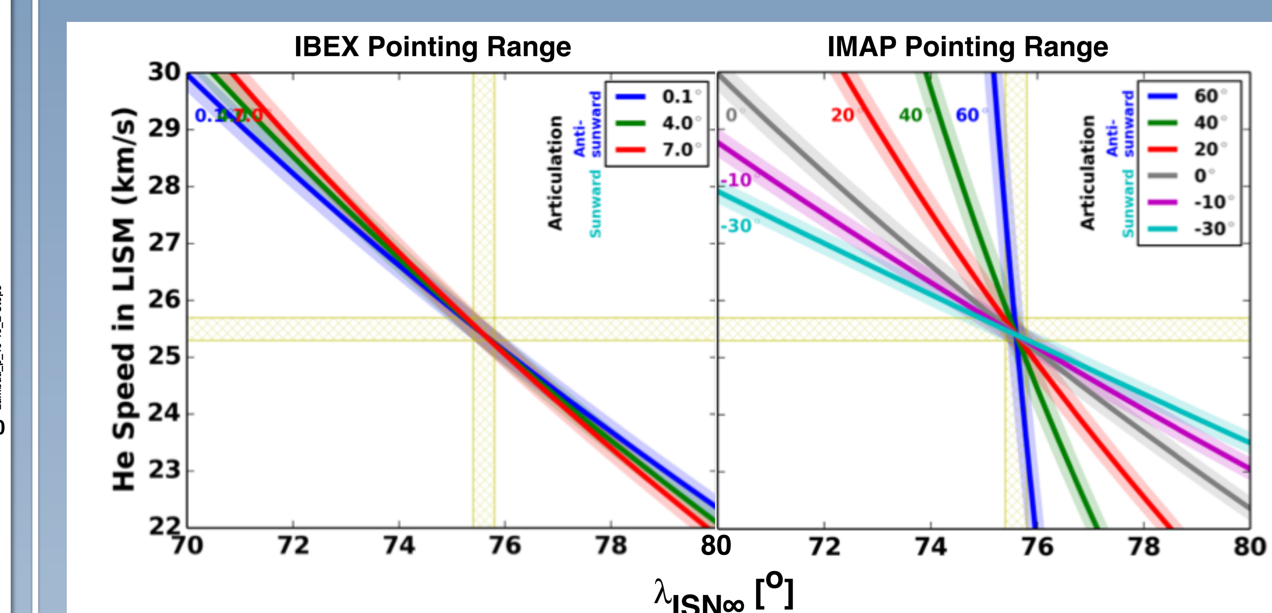

FIGURE 8: Following $\lambda_{ISN\ Peak}$ with different offsets of the spin axis ε_E from exact Sun-pointing provides different ISN parameter tubes according to eq. 1).
Left: Range of parameter tubes accessible with IBEX.
Right: Available range of parameter tubes with IMAP-Lo Pivot Platform.

Conclusions & Outlook

- **IBEX Viewing of ISN Flow Near Perihelion at 1 AU**
  Leads to 4-D ISN Parameter Tube, shown as $V_{ISN\infty}$, $\beta_{ISN\infty}$, $T_{ISN}(\lambda_{ISN\infty})$
  With small error bar across and large error bar along the tube
- **Parameter Tube Determined by ISN Flow Peak Location $\lambda_{ISN\ Peak}$**
  + Separate determination of $\lambda_{ISN\infty}$, e.g. from pickup ion cut-off [16]
- **Drivers that Help Break this IBEX Degeneracy**
  1) Latitude Peak Variation with Observer Longitude
  2) Latitude Width Variation with Observer Longitude
  3) Longitude Peak as Function of Offset ε_E from Sun-Pointing
  All Drivers contribute to full Chi-squared Optimization [1, 5]
- **1) & 3) Can be Used as Standalone Methods**
- $\lambda_{ISN\ Peak}$ **were Obtained for ISN He in All 4 ESA-Steps**
  → E-Dependence of Efficiency: Constant in E3 (55 eV), almost in E1 & 2
  → ESA Step 3 for variation of $\lambda_{ISN\ Peak}$ with offset from Sun-Pointing ε_E
- **IBEX Provides Only Weak Constraint on $\lambda_{ISN\infty}$ with Its Pointing Range**
  Because of advent of IMAP:
  → Reduce IBEX Sun-Pointing variation & concentrate on Time Evolution
- **Full Pointing Range Available with IMAP-Lo Pivot Platform!**
- **IMAP will also have Pickup Ion Observations**
  → **Allows Additional Consistency Check on $\lambda_{ISN\infty}$**

References

1. M. Bzowski et al., *Astrophys. J. Supp.* **220**:28 (2015).
2. T. Leonard et al., *Astrophys. J.* **804**:42 (2015).
3. D. J. McComas et al., *Astrophys. J. Supp.* **220**:22 (2015).
4. E. Möbius et al., *Astrophys. J. Supp.* **220**:24 (2015).
5. N.A. Schwadron et al., *Astrophys. J. Supp.* **220**:25 (2015).
6. M. Witte, *Astron. & Astrophys.* **426**, 835 (2004).
7. M. Bzowski et al., *Astron. & Astrophys.* **569**, A8 (2014).
8. B. Wood, H.-R. Mueller & M. Witte, *Astrophys. J.* **801**:62 (2015).
9. N.A. Schwadron et al., *Science* **343**, 988 (2014).
10. R. Lallement et al., *Science* **307**, 1447 (2005).
11. V. Izmodenov, D. Alexashov & A. Myasnikov, *Astron. & Astrophys.* **437**, L35 (2005).
12. P.C. Frisch et al., *Science* **341**, 1080 (2013).
13. P.C. Frisch et al., *Astrophys. J.* **801**:61 (2015).
14. R. Lallement & J.-L. Bertaux, *Astron. & Astrophys.* **565**, A41 (2014).
15. M. A. Lee, E. Möbius & T. Leonard, *Astrophys. J. Supp.* **220**:23 (2015).
16. E. Möbius, M. A. Lee & C. Drews, *Astrophys. J.* **815**:20 (2015).
17. A. Taut et al., *Astron. & Astrophys.*, **611**, A61 (2018).
18. E. Möbius et al., *Astrophys. J. Supp.* **198**:11 (2012).
19. M.A. Kubiak et al., *Astrophys. J. Supp.* **223**:25 (2016).